RSC Advances

ROYAL SOCIETY OF CHEMISTRY

www.rsc.org/advances

ARTICLE TYPE www. rsc.org/xxxxxx | XXXXXXXX

Enhancement of photocatalytic activity of two-dimensional GeH/graphene heterobilayer under visible light

Hao Jin,[a,b] Ying Dai,*[a] Xiang-Chao Ma,[a] Lin Yu,[a] Wei Wei,[a] and Bai-Biao Huang[a]

Received Xth XXXXXXXXXX 20XX, Accepted Xth XXXXXXXXX 20XX
First published on the web Xth XXXXXXXXXX 200X
DOI: 10.1039/b000000x

Searching for novel photocatalysts is one of the most important topic in photocatalytic fields. For this purpose, in the present work, the structural, electronic, and optical properties of GeH as well as GeH/graphene heterointerface are studied based on the hybrid density functional calculations including the nonlocal van der Waals correction. Our results show that the strain-engineered GeH monolayer will capture a broad range of the solar spectrum. Moreover, photogenerated electron-hole pairs can be efficiently separated in GeH/graphene heterojunction by formation of a Schottky barrier. Comparing to a pure GeH monolayer, the hybrid GeH/graphene complex displays an enhanced optical absorption in the visible region, suggesting powerful potentials in energy and environmental applications.

1 Introduction

In the last several decades, great efforts have been made to extend the light absorption spectra of photocatalysts, e.g. TiO_2, to the visible range by doping metal ions and/or non-metal ions.[1–4] However, the photocatalytic activity of doped materials would be impaired by the thermal instability or the formation of carrier recombination centres due to the strong localized states within the band gap.[4,5] To overcome the disadvantages of doping, composite photocatalysts were developed based on the energy exchange between materials with different electronic structures, which could efficiently separate photogenerated electron-hole pairs as well as modulate the band gap due to the combined effect of their heterolayered structure.[6–8] In addition, the emergence of two-dimensional (2D) materials (i.e. graphene and graphene-like materials) has opens up a new way to searching for efficient composite photocatalysts.[9–11] For example, Wang *et al*. demonstrated that a ZnO photocatalyst hybridized with graphite-like C_3N_4 exhibits high performance of photocatalytic activity and enhanced stability against photocorrosion due to the efficient charge separation.[12] Du and coworkers reported that the optical response of hybrid C_3N_4 and graphene composite is greatly enhanced in the visible-light region.[13]

Recently, Bianco *et al*. reported a novel graphene-like GeH, which has single-atom layers stacked 2D structure.[14] And its electron mobility is reported to be five time higher than that of bulk germanium and ten times higher than that of silicon, which is expected to have potential applications in photocatalysis.[15,16] Therefore, it is very interesting to study photocatalytic ability of GeH, as well as the combined effect of hybrid GeH and graphene nanocomposite. Unfortunately, to the best of our knowledge, both experimental and theoretical investigations on this issue are still scarce.

Based on the hybrid density functional calculations with the inclusion of the nonlocal van der Waals (vdW) correction, we here study the structural, electronic and optical properties of GeH as well as the GeH/graphene bilayer. The results demonstrate that GeH has a tunable band gap by isotropic strain, which is suitable for visible and even infrared adsorption. However it shows relatively low photocatalytic activity due to the high recombination rate of the charge carriers. Nevertheless, our investigation demonstrate that the introduced GeH/graphene heterointerface can not only promote the separation of photogenerated charge carriers with the formation of a Schottky barrier, but also enhance the optical response under visible-light region, enabling the development of more efficient visible-light driven photocatalysts.

2 Computational Methods

Our DFT calculations were carried out using the Vienna *ab initio* simulation package (VASP),[17,18] with projector augmented wave (PAW) method,[19] and the Perdew-Burke-Ernzerhof (PBE) generalized gradient approximation (GGA) to the exchange correlation functional.[20] To account for the underestimation of the band gap in standard DFT calculations, the accurate electronic structures were calculated using the Heyd-Scuseria-Ernzerhof (HSE06) hybrid functional,[21,22] in which the hybrid functional is mixed with 25% exact Hartree-

[a] *School of Physics, State Key Laboratory of Crystal Materials, Jinan, 250100, People's Republic of China. E-mail: daiy60@sina.com*
[b] *Department of Materials Engineering, The University of British Columbia, Vancouver, BC, Canada V6T 1Z4*

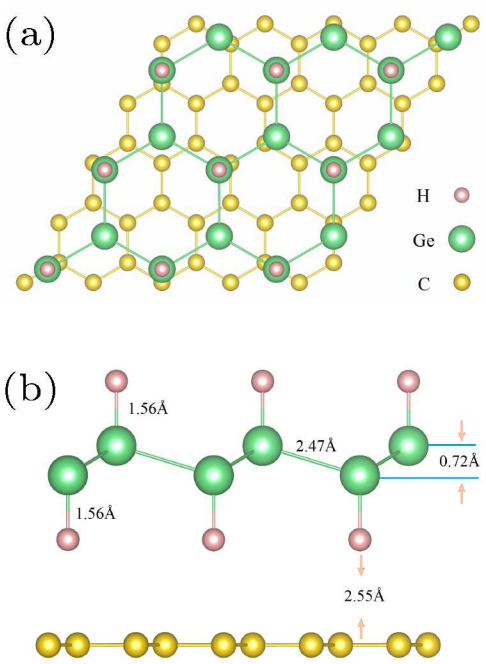

Fig. 1 Optimized structures of GeH/graphene heterojunction. (a) Top view, and (b) side view.

Fock (HF) exchange. A damped vdW correction based on Grimme's scheme is also incorporated to better describe the nonbonding interaction between GeH and graphene monolayer.[23]

A cutoff energy of 500 eV was used to truncate the plane-wave expansion of the wave functions. The first Brillouin zone is sampled with Monkhorst-Pack grid of 5×5×1 for structure optimization and 9×9×1 for static calculation.[24] The vacuum space is set to be 20 Å, which is large enough to avoid interactions between periodic images. The atomic positions were fully relaxed in all reported calculations using the conjugate gradient (CG) method to an energy convergence of 10^{-6} eV and force convergence of 10^{-2} eV/Å.

In order to simulate the hybrid GeH/graphene nanocomposite, a 5×5 graphene supercell with the dimension of 12.3×12.3 $Å^2$ is used, which perfectly matches with a 3×3 GeH supercell. The optimized structures for hybrid GeH/graphene complex are present in Figure 1.

The binding energy between the monolayer GeH and graphene was obtained according to the following equation:

$$E_b = \frac{1}{A_s}(E_{gC} + E_{GeH} - E_{gC+GeH}) \quad (1)$$

where E_{C+GeH}, E_{gC}, and E_{GeH} represent the total energy of the relaxed hybrid GeH/graphene complex, the pure graphene sheet, and a GeH monolayer, respectively. A_s refers to the area of the heterointerface. Note that a positive value indicates favorite binding.

To calculate the optical properties of GeH/graphene nanocomposite, the frequency-dependent dielectric matrix is determined with HSE06 functional. The imaginary part is calculated by a summation over empty states using the equation:[25]

$$\varepsilon_2^{\alpha\beta}(\omega) = \frac{4\pi^2 e^2}{\Omega} \lim_{q\to 0} \frac{1}{q^2} \sum_{c,v,\boldsymbol{k}} 2\omega_{\boldsymbol{k}} \delta(\varepsilon_{c\boldsymbol{k}} - \varepsilon_{v\boldsymbol{k}} - \omega) \times \langle \mu_{c\boldsymbol{k}+q\boldsymbol{e}_\alpha} | \mu_{v\boldsymbol{k}} \rangle \langle \mu_{v\boldsymbol{k}} | \mu_{c\boldsymbol{k}+q\boldsymbol{e}_\beta} \rangle \quad (2)$$

where the indices c and v refer to conduction and valence band states, respectively. $\mu_{c\boldsymbol{k}}$ represents the cell periodic part of the wavefunctions at the k point.The real part of the dielectric tensor $\varepsilon_1(\omega)$ is then obtained by a Kramers-Kronig transformation. The absorption coefficient ($\alpha(E)$) is then evaluated according to the following expression:[26]

$$\alpha(E) = \frac{4\pi e}{hc} \{ \frac{[\varepsilon_1^2 + \varepsilon_2^2]^{1/2} - \varepsilon_1}{2} \}^{1/2} \quad (3)$$

3 Results and Discussion

As shown in Figure 1, the germanium atoms form a honeycomb structure with the buckling of the germanium plane of 0.72 Å. The hydrogen atoms bond to the Ge atoms on both sides of the plane in an alternating manner. The Ge-Ge and Ge-H bond length are 2.47 Å and 1.56 Å, respectively. The equilibrium distance between graphene monolayer and GeH is calculated to be 2.55 Å. The heterointerface binding energy is obtained according to Equation 1 with the value of 0.84 J/m^2. This value is about 3 times larger than that of the graphene/g-C_3N_4 complex,[13] and one order of magnitude larger when compared with the GeH/TiO_2(101) composite,[15] indicating a very high stability.

In order to understand the prospective photocatalytic performance of GeH/graphene heterojunctions, we first studied the electronic structures of GeH monolayer using hybrid functional calculations. The band structures of GeH are shown in Figure 2(a). It can be seen that GeH monolayer has a direct band gap of 1.61 eV at Γ, in good agreement with recent experiments.[14,16] In addition, the results of band edge positions suggest that GeH has suitable redox potentials, with the oxidation potential (V_{O_2/H_2O}) slightly below the valence band, while the reduction level (V_{H^+/H_2}) in between the gap.

Previous studies have demonstrated that tensile stress could drive GeH monolayer into a topological insulator (TI).[27,28] To better understand the influence of the strain on photocatalytic

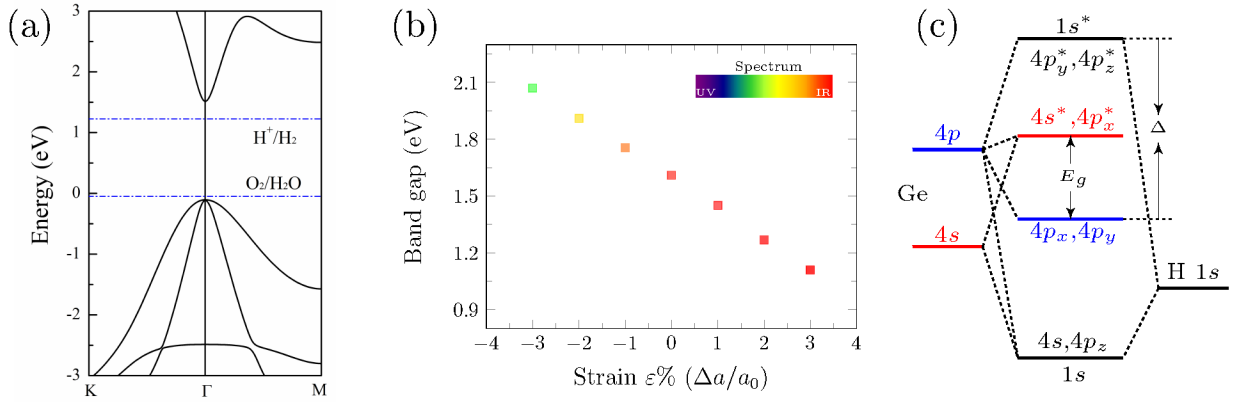

Fig. 2 (a) The band structure of GeH using HSE06 functional. The redox potentials are indicated by the blue dashed lines. The Fermi Level is set to zero. (b) The calculated band gaps of GeH monolayer as a function of strain. (c) Schematic diagram of the energy levels at Γ for GeH. The superscript "*" refers to the antibonding states.

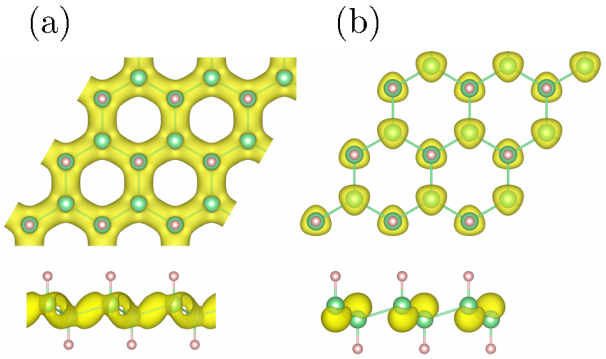

Fig. 3 The charge distribution of (a) valence band and (b) conduction band at Γ with isovalue of 0.01 e/Å^3.

response, here we investigate the strain dependence of band gap of GeH monolayer. The tensile or compressive stress is uniformly applied and the crystal symmetries are maintained. The isotropic strain is defined as $\varepsilon = \Delta a/a_0$, where the lattice constants of strained and unstrained supercells refer to $a_0 + \Delta a$ and a_0, respectively. The calculated band gaps as a function of strain are plotted in Figure 2(b).

The results show that when tensile stress is applied, Ge-Ge bonding is weakened due to the increased bond length, hence the splitting of bonding and antibonding states is decreased, leading to the reduction of the band gap. If the tensile stress is high enough, the valence band maximum (VBM) and conduction band minimum (CBM) of GeH degenerate at the Fermi level at Γ, and the system becomes a semimetal.[27] In contrast, when the system undergoes compression, the splitting of bonding and antibonding states is increased linearly, giving rise to the larger band gap. Consequently, our results show that the strain-engineered GeH monolayer will capture a broad range of the solar spectrum.

Despite these advanced properties, there are also some drawbacks for GeH. As shown in Figure 2(c), VBM is mainly composed of Ge 4p orbitals, whereas the CBM is composed of the Ge 4s and 4p mixed states. The charge density distribution of VBM and CBM is largely overlapped (see Figure 3). As a result, the photoexcited electrons have high possibilities to fall back to the valence band, leading to low photocatalytic activity. The high recombination rate of the photogenerated electron-hole pairs hinders the practical applications of GeH. To overcome this problem, a GeH/graphene heterostructure is employed.

Upon formation of the interface, our calculations suggest a redistribution of the ground state charge in the system. In Figure 4(a) and (b), the three-dimensional charge density difference are plotted, which are obtained by subtracting the charge density of the hybrid GeH/graphene complex from that of the independent GeH and graphene monolayers. It can be clear seen that there is a space charge region within the GeH/graphene heterointerface. This can be understood based on the fact that hydrogen has a strong ability to attract the extra electrons. When graphene adheres to the GeH monolayer, the interaction between carbon and hydrogen atoms exerts a driving force, which leads to the electrons transfer from the

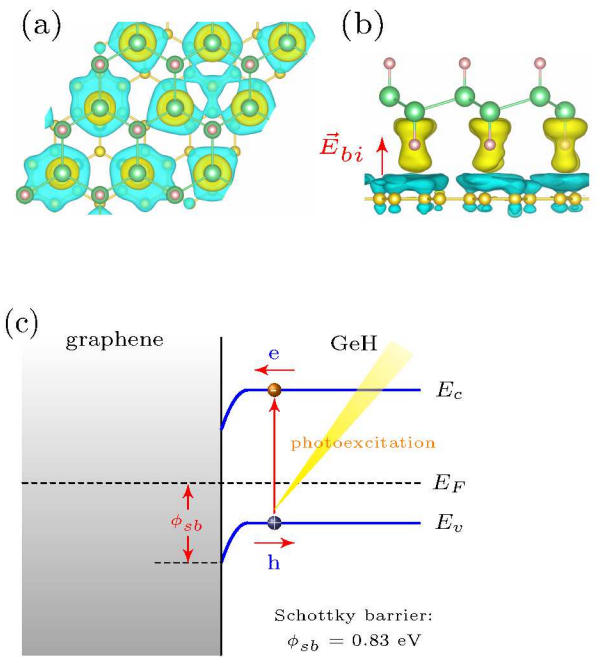

Fig. 4 (a) Top and (b) side view of the three-dimensional charge density difference at the GeH/graphene heterointerface. Yellow and light blue isosurfaces represent charge accumulation and depletion with isovalue of 0.001 e/Å^3. (c) Band alignment at a GeH/graphene interface. ϕ_{sb} is the hole Schottky barrier.

areas of graphene to the areas of GeH monolayer, while holes move in the opposite way. As shown in Figure 4(b), when the charge redistribution in the GeH/graphene heterointerface reaches equilibrium, a built-in electric field ($\vec{E}_{bi}$) is induced. Since graphene is a semimetal and GeH is a semiconductor, the space charge region of GeH/graphene heterointerface results in the formation of a Schottky barrier (ϕ_{sb}). The band bending associated with the Schottky barrier height is illustrated in Figure 4(c).

To better understand the interface involved, we analyzed the band alignment and calculated the Schottky barriers by employing the lineup method.[29,30] In the first step, we determined the work functions of GeH and graphene monolayers, which are determined as the difference between the vacuum level and the Fermi energy. Based on the hybrid DFT results, the calculated work function of graphene is 4.54 eV, in good agreement with measured values in the range of 4.3∼4.6 eV.[9,10] The work function of GeH monolayer is 5.64 eV, about 24% larger than that of graphene. The Schottky barrier at the GeH/graphene heterointerface was then determined as the difference between the Fermi energy of the bilayer and the

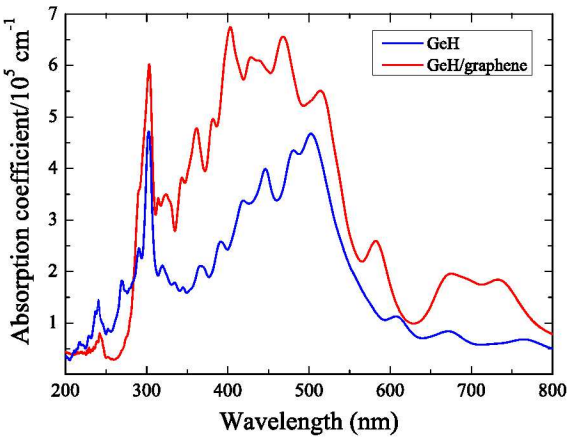

Fig. 5 The calculated optical absorption for GeH monolayer and GeH/graphene complex as a function of wavelength.

VBM energy in an isolated GeH monolayer, corrected by the interface dipole potential as detailed in the work by Shan *et al.*.[29] The calculated ϕ_{sb} is 0.83 eV for holes to diffuse from graphene to GeH. Thus, when charge carriers are photoexcited, photogenerated holes in the valence band of GeH are trapped due to the Schottky barrier whereas the photogenerated electrons can freely diffuse from the conduction band of GeH to graphene (see Figure 4(c)). Therefore, photoexcited charge carriers can be separated effectively at GeH/graphene heterojunctions, which lead to higher energy utilization efficiency and improve the photocatalytic performance.

In order to investigate the visible-light adsorption ability of GeH/graphene heterointerface, we calculated the optical absorption spectrum, which are obtained by Equation 3. As shown in Figure 5, we found that HSE06-computed results can successfully reproduce the experimentally observed optical absorption spectrum of GeH monolayer.[16] Our calculations demonstrate that the GeH/graphene bilayer shows an enhanced absorption, with the integrated intensity up to 2 times larger than the GeH monolayer. In addition, the absorption spectrum of such hybrid complex has been expanded into the orange-red region of the visible spectrum comparing with the pure GeH monolayer, indicating that the hybrid GeH/graphene nanocomposite could harvest a broader range of visible light efficiently.

4 Conclusion

In this work, the structural and electronic properties of GeH as well as its band alignment with graphene were studied using hybrid functional DFT calculations with the inclusion of the nonlocal vdW correction. Our results demonstrate that the strain-engineered GeH monolayer will capture a broad

range of the solar spectrum. Moreover, the interactions within the hybrid GeH/graphene complex lead to the charge redistribution, which induce the built-in electric field and form a Schottky barrier. Further analysis indicates that such heterointerface could be beneficial to facilitate the photogenerated charge separation, and enhance the optical response of GeH monolayer under visible-light region. Thus, it is proposed that GeH/graphene composite may be a powerful visible-light driven photocatalyst.

Acknowledgements

This work is supported by the National Basic Research Program of China (973 program, 2013CB632401), National Natural Science foundation of China under Grants 21333006 and 11374190, and the Fund for Doctoral Program of National Education 20120131110066.

References

1 R. Asahi, T. Morikawa, T. Ohwaki, K. Aoki and Y. Taga, *Science*, 2001, **293**, 269–271.
2 S. Khan, M. Al-Shahry and W. Ingler, *Science*, 2002, **297**, 2243–2245.
3 H. Jin, Y. Dai, W. Wei and B.-B. Huang, *J. Phys. D: Appl. Phys.*, 2008, **41**, 195411.
4 Z. Wang, Y. Liu, B. Huang, Y. Dai, Z. Lou, G. Wang, X. Zhang and X. Qin, *Phys. Chem. Chem. Phys.*, 2014, **16**, 2758–2774.
5 W. Choi, A. Termin and M. R. Hoffmann, *J. Phys. Chem.*, 1994, **98**, 13669–13679.
6 W. Wang, B. Huang, X. Ma, Z. Wang, X. Qin, X. Zhang, Y. Dai and M.-H. Whangbo, *Chem. Eur. J.*, 2013, **19**, 14777–14780.
7 H. Cheng, B. Huang, P. Wang, Z. Wang, Z. Lou, J. Wang, X. Qin, X. Zhang and Y. Dai, *Chem. Commun.*, 2011, **47**, 7054–7056.
8 R. Zhang, Y. Dai, Z. Lou, Z. Li, Z. Wang, Y. Yang, X. Qin, X. Zhang and B. Huang, *CrystEngComm*, 2014, **16**, 4931–4934.
9 Q. Tang and Z. Zhou, *Prog. Mater. Sci.*, 2013, **58**, 1244 – 1315.
10 G. Xie, K. Zhang, B. Guo, Q. Liu, L. Fang and J. R. Gong, *Adv. Mater.*, 2013, **25**, 3820–3839.
11 Y. Ma, Y. Dai, M. Guo and B. Huang, *Phys. Rev. B*, 2012, **85**, 235448.
12 Y. Wang, R. Shi, J. Lin and Y. Zhu, *Energy Environ. Sci.*, 2011, **4**, 2922–2929.
13 A. Du, S. Sanvito, Z. Li, D. Wang, Y. Jiao, T. Liao, Q. Sun, Y. H. Ng, Z. Zhu, R. Amal and S. C. Smith, *J. Am. Chem. Soc.*, 2012, **134**, 4393–4397.
14 E. Bianco, S. Butler, S. Jiang, O. D. Restrepo, W. Windl and J. E. Goldberger, *ACS Nano*, 2013, **7**, 4414–4421.
15 M. Niu, D. Cheng and D. Cao, *Sci. Rep.*, 2014, **4**, 4810.
16 Z. Liu, Z. Lou, Z. Li, G. Wang, Z. Wang, Y. Liu, B. Huang, S. Xia, X. Qin, X. Zhang and Y. Dai, *Chem. Commun.*, 2014, **50**, 11046–11048.
17 G. Kresse and J. Furthmüller, *Phys. Rev. B*, 1996, **54**, 11169–11186.
18 G. Kresse and J. Furthmüller, *Comput. Mater. Sci.*, 1996, **6**, 15 – 50.
19 G. Kresse and D. Joubert, *Phys. Rev. B*, 1999, **59**, 1758–1775.
20 J. P. Perdew, K. Burke and M. Ernzerhof, *Phys. Rev. Lett.*, 1996, **77**, 3865–3868.
21 J. Heyd, G. Scuseria and M. Ernzerhof, *J. Chem. Phys.*, 2003, **118**, 8207–8215.
22 J. Paier, M. Marsman, K. Hummer, G. Kresse, I. C. Gerber and J. G. Ángyán, *J. Chem. Phys.*, 2006, **124**, 154709.
23 S. Grimme, *J. Comput. Chem.*, 2006, **27**, 1787–1799.
24 H. J. Monkhorst and J. D. Pack, *Phys. Rev. B*, 1976, **13**, 5188–5192.
25 M. Gajdoš, K. Hummer, G. Kresse, J. Furthmüller and F. Bechstedt, *Phys. Rev. B*, 2006, **73**, 045112.
26 X. Li, J. Zhao and J. Yang, *Sci. Rep.*, 2013, **3**, year.
27 C. Si, J. Liu, Y. Xu, J. Wu, B.-L. Gu and W. Duan, *Phys. Rev. B*, 2014, **89**, 115429.
28 Y. Ma, Y. Dai, C. Niu and B. Huang, *J. Mater. Chem.*, 2012, **22**, 12587–12591.
29 B. Shan and K. Cho, *Phys. Rev. B*, 2004, **70**, 233405.
30 M. Bernardi, M. Palummo and J. C. Grossman, *Nano Lett.*, 2013, **13**, 3664–3670.